Supplement of Atmos. Chem. Phys., 24, 2287–2318, 2024
https://doi.org/10.5194/acp-24-2287-2024-supplement

Atmospheric Chemistry and Physics
Open Access
EGU

Supplement of

A new process-based and scale-aware desert dust emission scheme for global climate models – Part II: Evaluation in the Community Earth System Model version 2 (CESM2)

Danny M. Leung et al.

Correspondence to: Danny M. Leung (dannymleung@ucla.edu)

Section S1. Significance in correlation differences.

For Fig. 10f, we use Fisher's Z transformation (Fisher, 1992) to test how significant a Pearson correlation coefficient is different from another. To compute a 2-tailed p-value of difference in correlations, the computation is a function of the two correlations (e.g., MIDAS DAOD vs. our scheme's DAOD as R_1; MIDAS DAOD vs. Z03's DAOD as R_2) and the sample size (for each grid, 2004–2008 daily data are in total $n_1 = n_2 = 1827$):

$$Z_1 = 0.5\ln\left(\frac{1+R_1}{1-R_1}\right) \quad \text{(S1)}$$

$$Z_2 = 0.5\ln\left(\frac{1+R_2}{1-R_2}\right) \quad \text{(S2)}$$

$$\text{score} = \frac{Z_1 - Z_2}{\sqrt{\frac{1}{n_1-3}+\frac{1}{n_2-3}}} \quad \text{(S3)}$$

Then we use the look up table to yield the p-value for the score. For computers,

$$p\ \text{value} = 2 \times \text{pnorm}(\text{abs}(\text{score})) \quad \text{(S4)}$$

Then, for instance,

If $R_1 = 0.45, R_2 = 0.4$, then p-value ~ 0.065 > 0.05;

If $R_1 = 0.65, R_2 = 0.6$, then p-value ~ 0.013 < 0.05;

If $R_1 = 0.85, R_2 = 0.8$, then p-value ~ 10^{-6} << 0.05.

Comparing with other maps of correlation differences in Figs. 6d-f with $|\Delta R|$ of 0.1–0.3, Fig. 10f overall has grids with much smaller $|\Delta R|$ values of < 0.02, which are not statistically significant. $|\Delta R|$ for any gridcell has to be > 0.082 to yield a p-value of < 0.05.

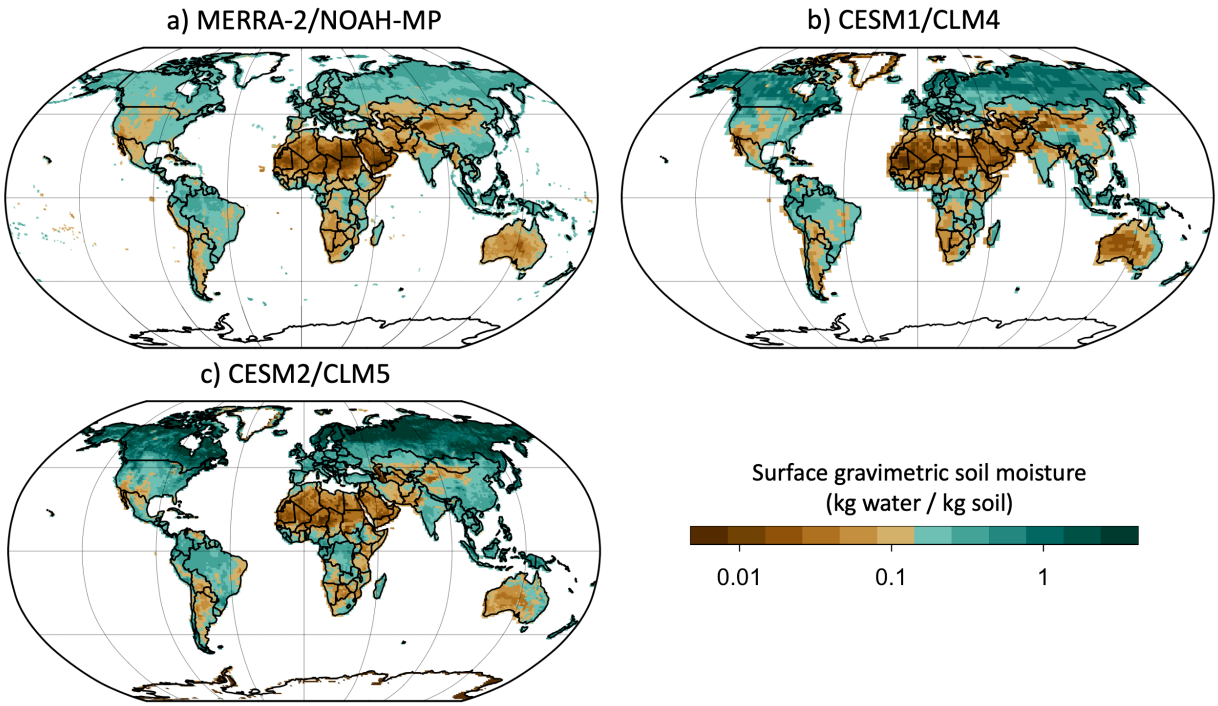

Figure S1. Gravimetric soil moisture for the topmost soil layer for (a) MERRA-2, (b) CLM4, and (c) CLM5.

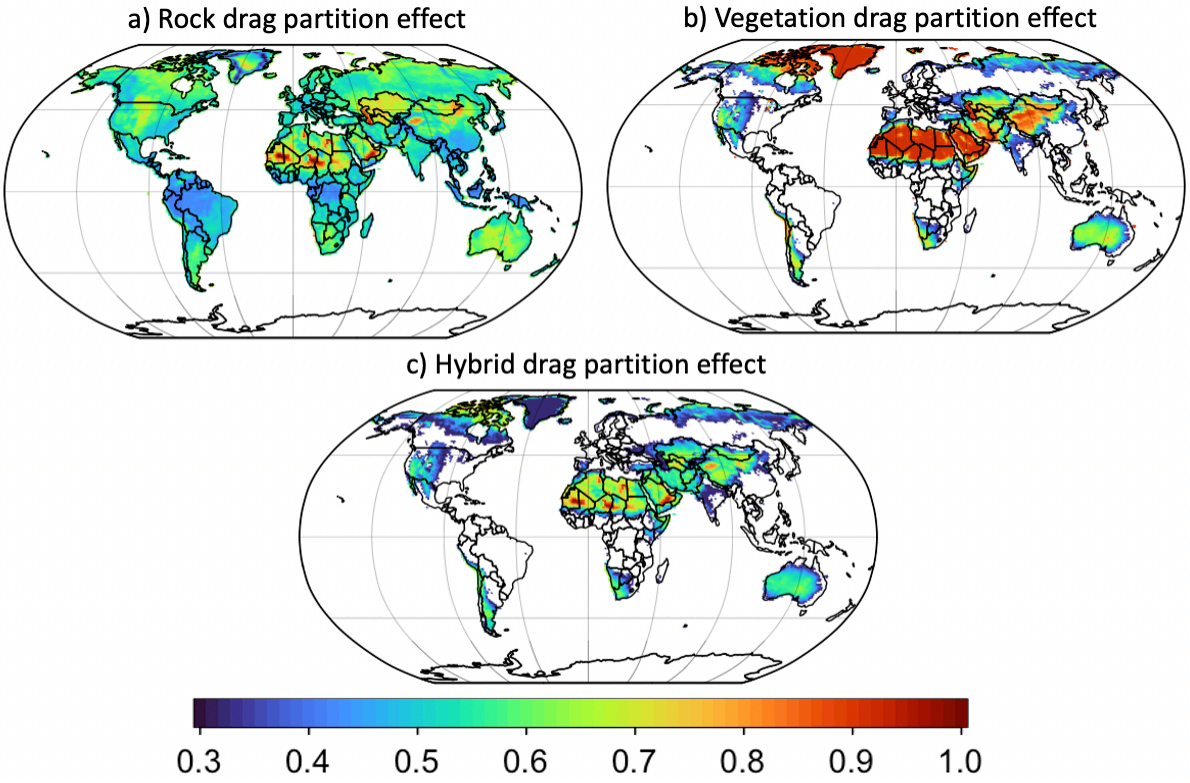

Figure S2. Drag partition effects due to (a) rocks, (b) green + brown vegetation, and (c) their combined effect.

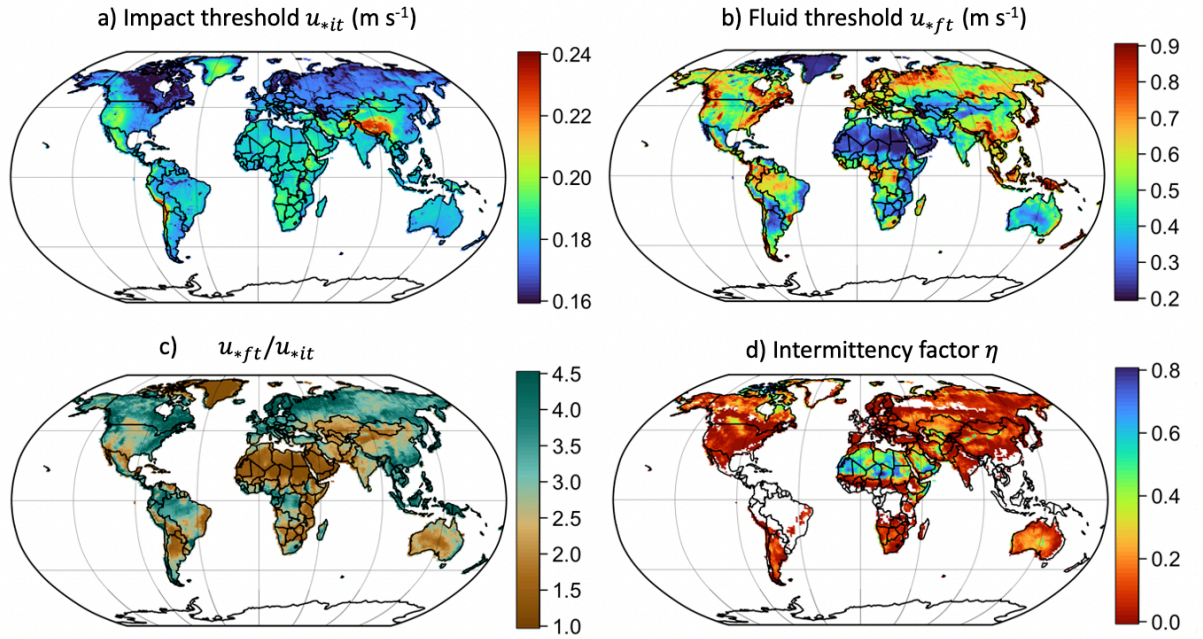

Figure S3. Dust emission thresholds and intermittency factor simulated by CLM5. (a) impact threshold friction velocity u_{*it}, (b) fluid threshold friction velocity u_{*ft}, (c) ratio of fluid to impact threshold u_{*ft}/u_{*it}, and (d) intermittency factor η for 2004–2008.

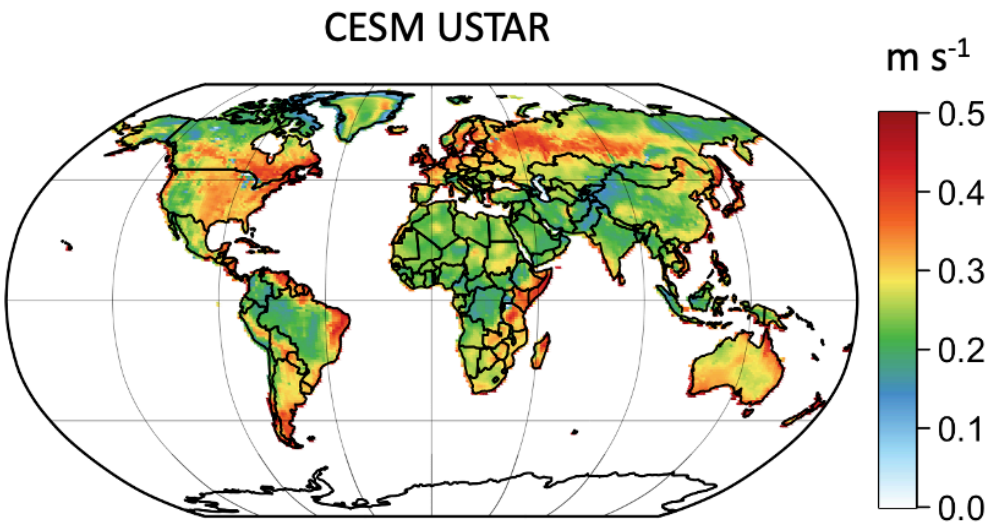

Figure S4. The CESM2 2004–2008 mean friction velocity u_* (m s^{-1}) for calculating dust emissions in CLM5. The wind comes from CAM6 with its meteorology nudged toward the MERRA-2 meteorology.

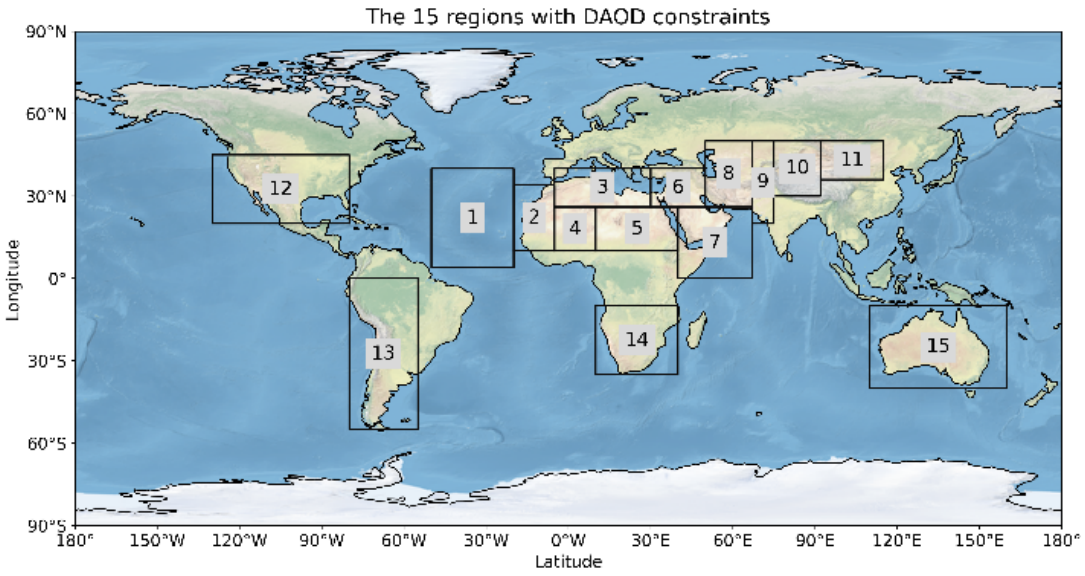

Figure S5. Coordinates of the 15 observed dusty regions with the Ridley et al. (2016) constraints on the regional DAOD. The coordinates of the 15 dusty regions are: (1) Mid-Atlantic (50–20°W; 4–40°N), (2) African west coast (20–5°W; 10–34°N), (3) Northern Africa (5°W–30°E; 26–40°N), (4) Mali / Niger (5°W–10°E; 10–26°N), (5) Bodélé / Sudan (10–40°E; 10–26°N), (6) Northern Middle East (30–50°E; 26–40°N), (7) Southern Middle East (40–67.5°E; 0–26°N), (8) Kyzylkum (50–67.5°E; 26–50°N), (9) Thar (67.5–75°E; 20–50°N), (10) Taklamakan (75–92.5°E; 30–50°N), (11) Gobi (92.5–115°E; 36–50°N), (12) North America (130–80°W; 20–45°N), (13) South America (80–55°W; 55–0°S), (14) Southern Africa (10–40°E; 35–10°S), and (15) Australia (110–160°E; 40–10°S). The figure is adapted from Kok et al. (2021).

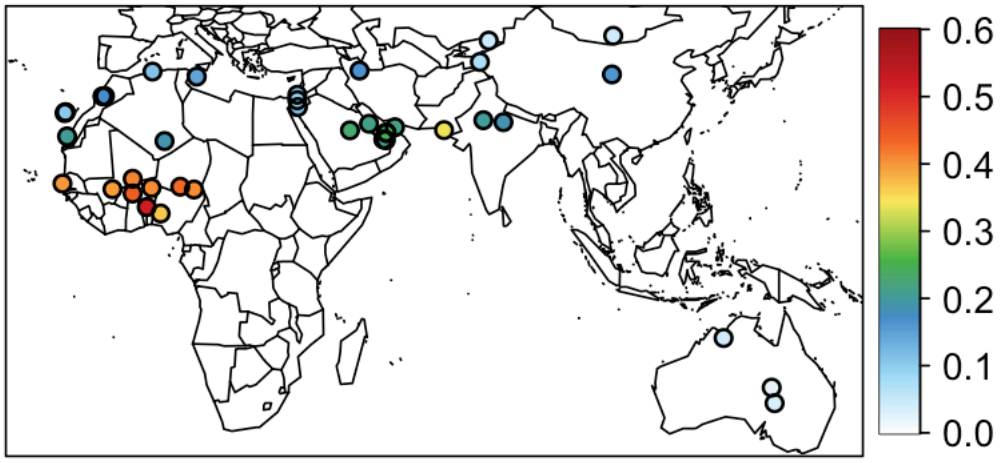

Figure S6. AERONET–SDA AOD, averaged across all available observations within years 2004–2008, for 39 selected dust-dominant AERONET stations following Kok et al. (2014b).

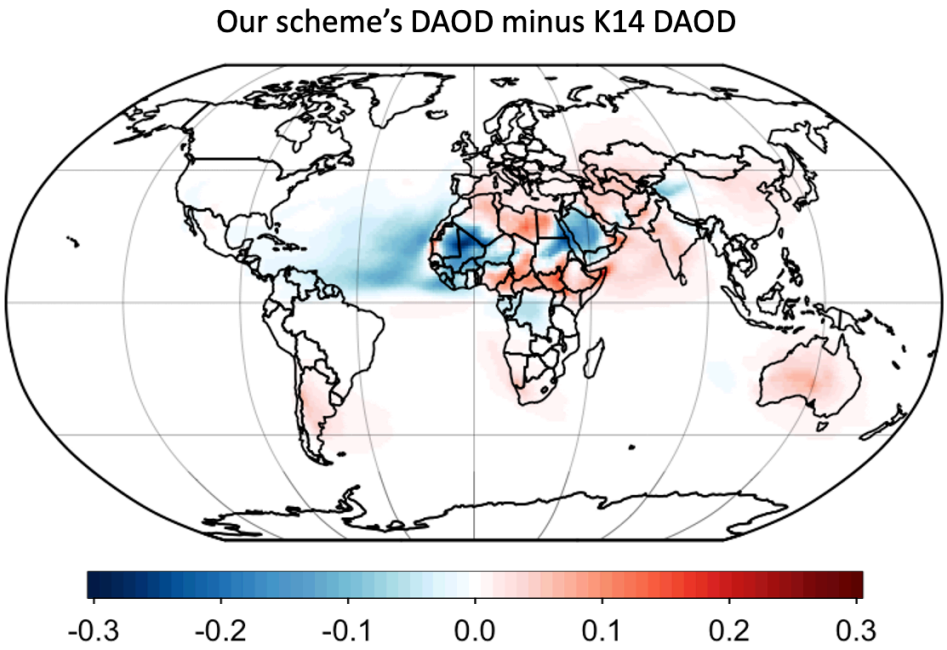

Figure S7. Global DAOD difference between our new scheme (Leung et al., 2022) and the K14 scheme, i.e., Fig. 3b minus Fig. 3a.

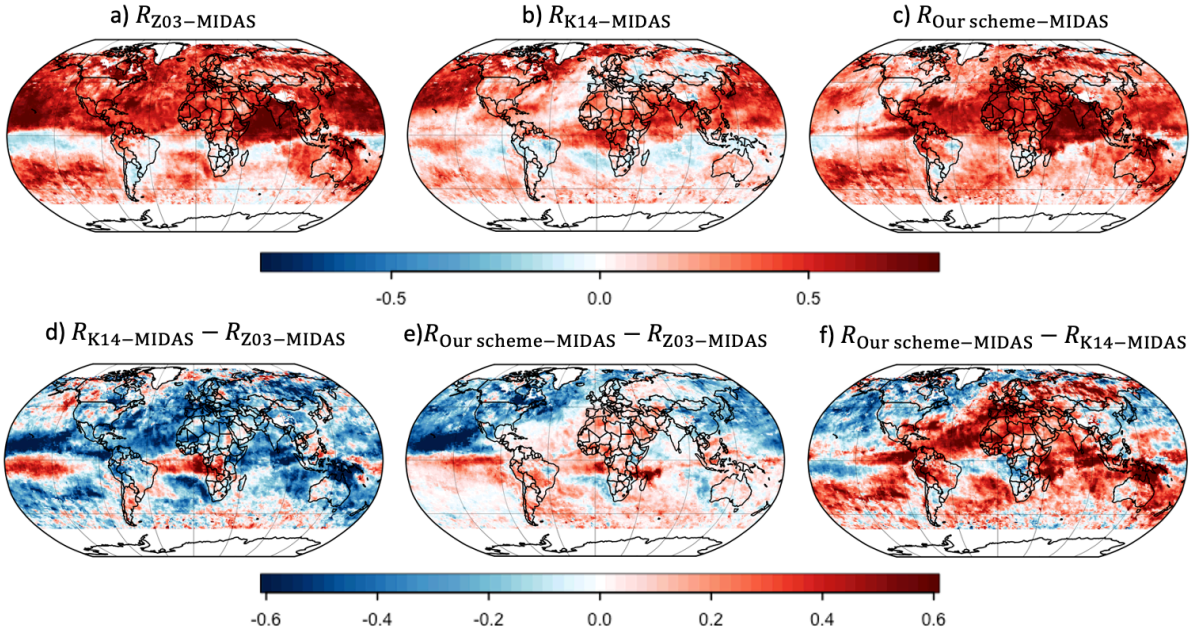

Figure S8. Grid-by-grid MIDAS DAOD daily correlation maps with CESM2 for 2004–2008. (a-c) Correlation maps R of MIDAS daily DAOD time series vs. CESM2 daily DAOD time series using (a) Z03, (b) K14, and (c) our scheme. The correlation maps focus on gridboxes with MIDAS DAOD/AOD ratio > 0.25 only. (d–f) Changes (ΔR) in correlation maps between CESM and MIDAS DAOD, from (d) Z03 to K14, (e) Z03 to our scheme, and from (f) K14 to our scheme. This figure is the same as Fig. 6 in the main text but no masking for low MIDAS DAOD / AOD values.

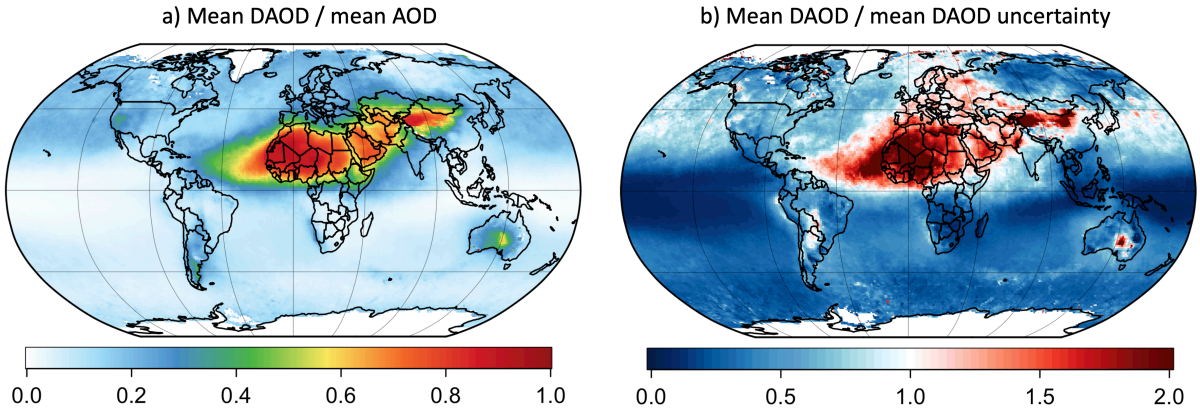

Figure S9. MIDAS (a) mean DAOD / mean total AOD values, and (b) ratio of mean DAOD / mean DAOD uncertainty (quantified by Gkikas et al., 2021), averaged across 2004–2008. Polar regions and snow/ice covered continents have no values.

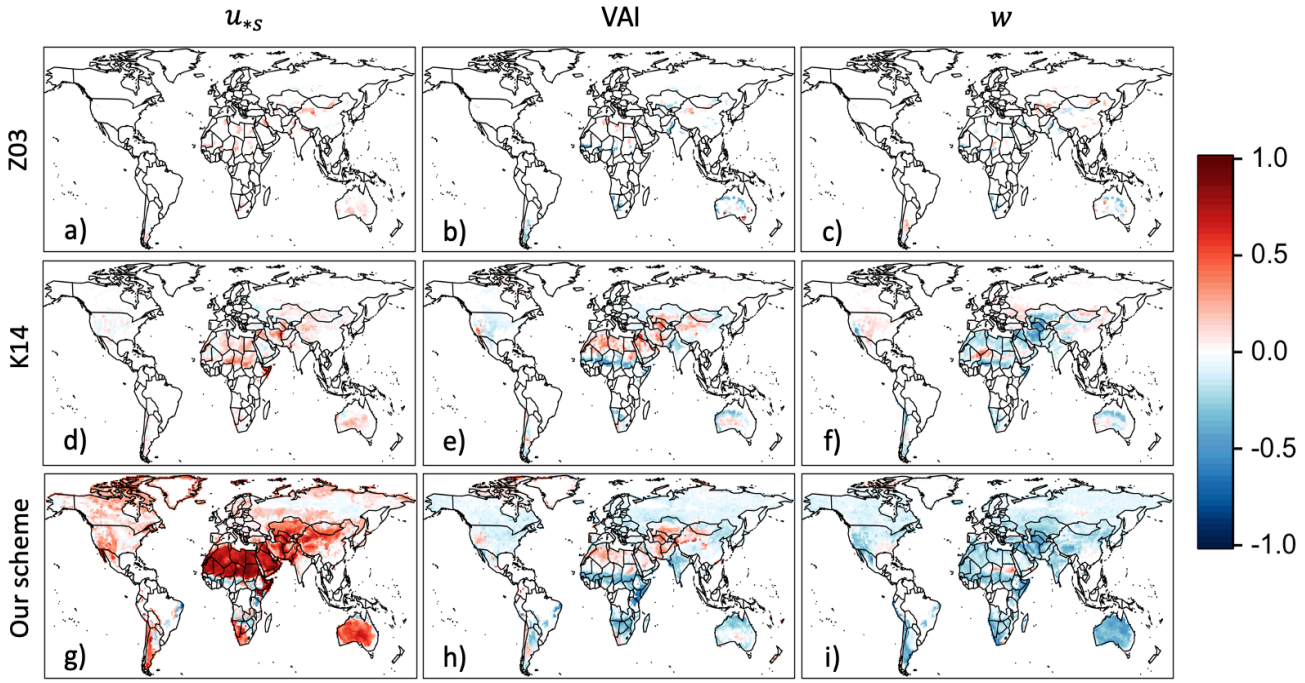

Figure S10. Grid-by-grid daily Pearson correlation maps between simulated dust emissions and the three fundamental driving meteorological fields in CESM2 for 2004–2008. Each row represents an emission scheme, including (a-c) Z03, (d-f) K14, and (g-i) our scheme. Each column represents a meteorological or land surface field in CESM2 that fundamentally drives dust emission, including soil surface friction velocity u_{*s} (m s^{-1}) as the left column (we use u_* for Z03 and K14), vegetation area index (VAI; m^2 plant / m^2 land) as the middle column, and soil moisture w (kg water / kg soil) as the right column.

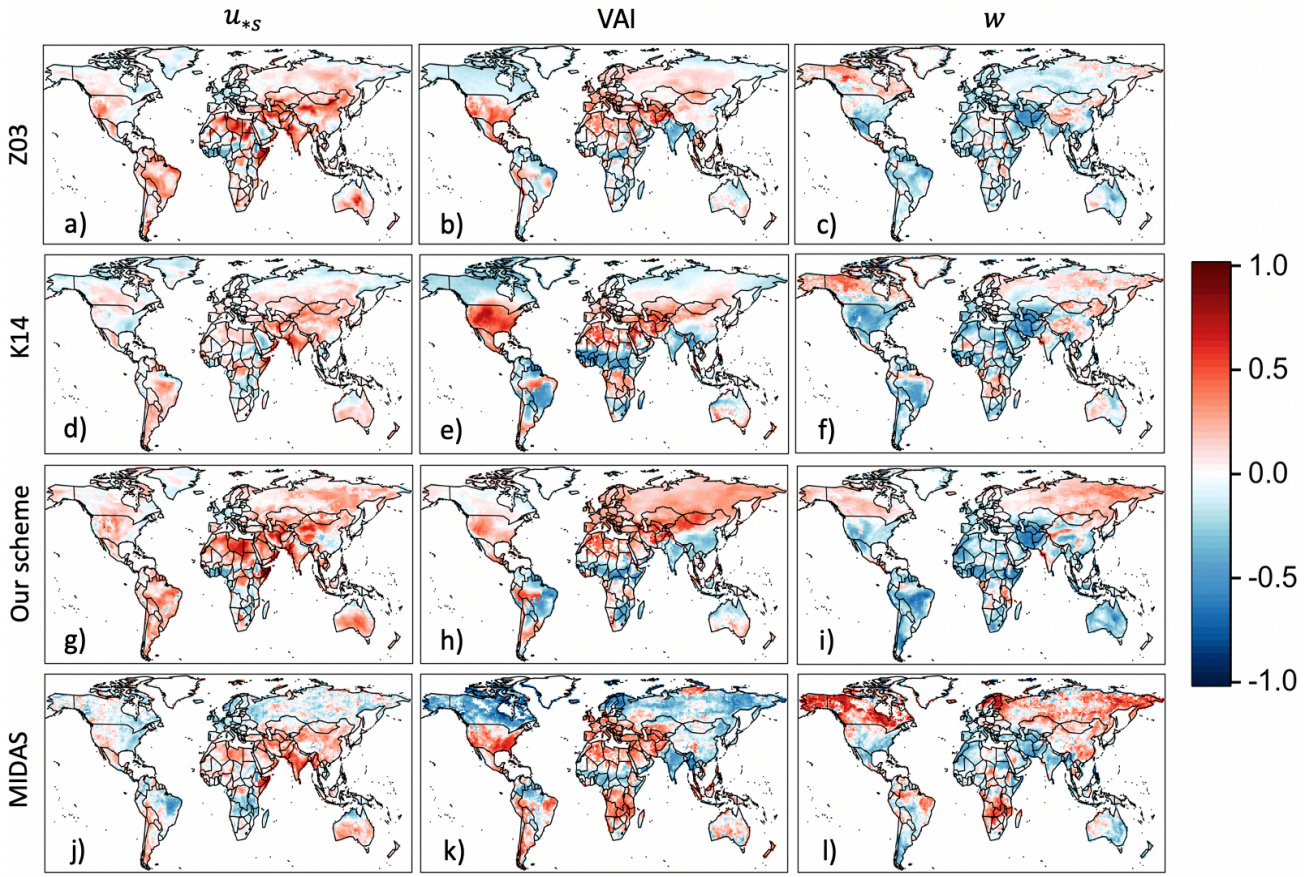

Figure S11. Grid-by-grid daily Pearson correlation maps between DAOD and the three fundamental driving meteorological fields in CESM2 for 2004–2008. The first three rows use the DAOD simulated using different emission schemes in CESM2, respectively (a-c) Z03, (d-f) K14, and (g-i) our scheme, and the last row uses MIDAS DAOD. Each column represents a meteorological or land surface field in CESM2 that fundamentally drives dust emission, including soil surface friction velocity u_{*s} (m s^{-1}) as the left column (we use u_* for Z03 and K14, and MIDAS), vegetation area index (VAI; m^2 plant / m^2 land) as the middle column, and soil moisture w (kg water / kg soil) as the right column. Note that the DAOD correlations do not cover the oceans because the meteorological and land surface fields used here are only defined over the continents.

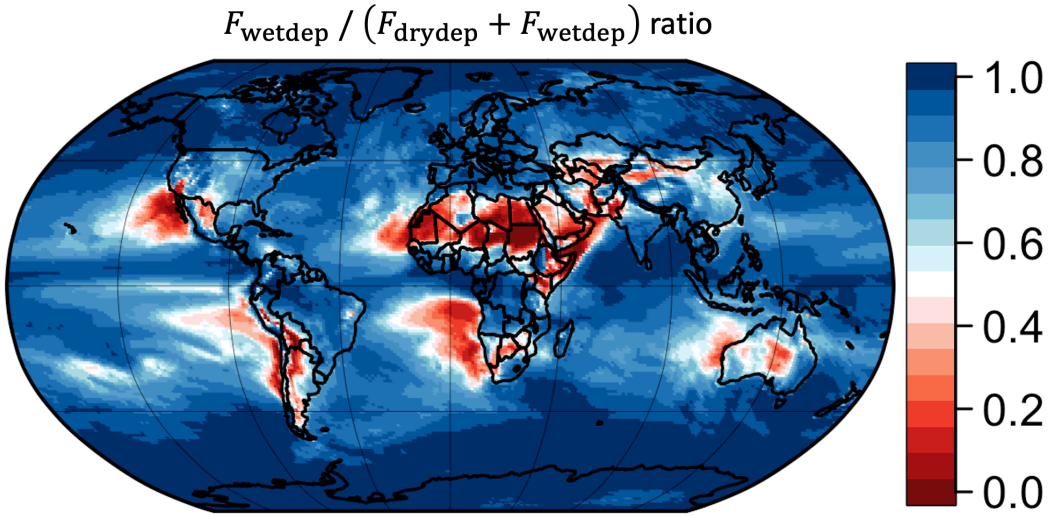

Figure S12. The fraction of wet dust deposition flux over the total (dry + wet) dust deposition flux, averaged across 2004–2008.

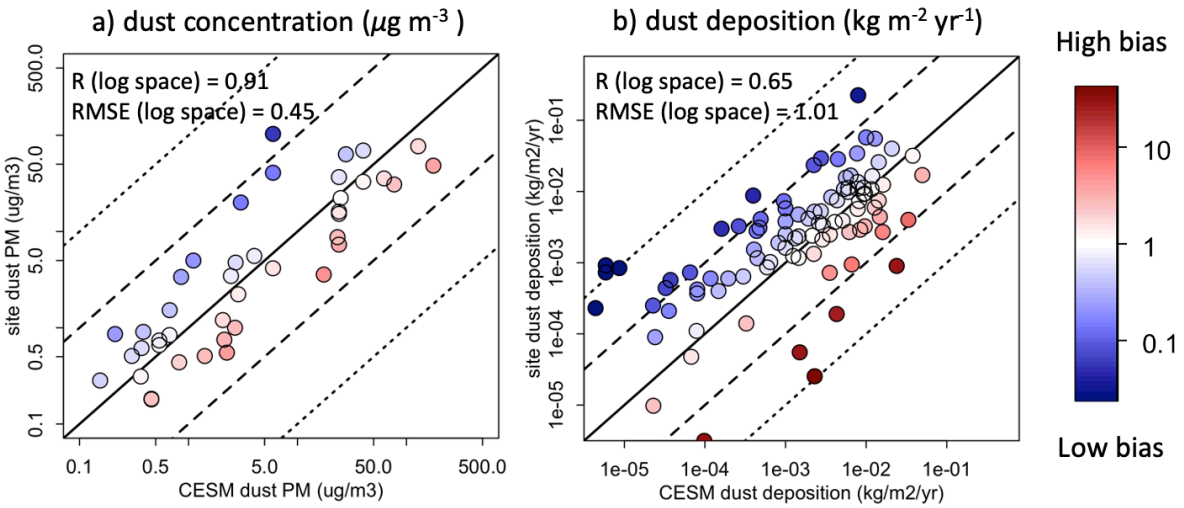

Figure S13. Our scheme's dust PM concentrations (in μg m^{-3}) and depositions (in kg m^{-2} yr^{-1}) after implementing the scaling map $\widetilde{K}_c$, versus site dust PM concentrations and depositions.

Table S1. AERONET station location information for 39 selected dust-dominant AERONET stations following Kok et al. (2014b).

Selected station name	Longitude	Latitude
Agoufou	-1.479117	15.34540
Bahrain	50.609267	26.20805
Banizoumbou	2.665190	13.54693
Birdsville	139.345960	-25.89893
Blida	2.880556	36.50833
DMN_Maine_Soroa	12.023067	13.21672
Dahkla	-15.950000	23.71667
Dakar	-16.958611	14.39417
Dalanzadgad	104.419167	43.57722
Dhabi	54.382778	24.48056
Dhadnah	56.324717	25.51282
Djougou	1.599010	9.76007
Eilat	34.917500	29.50250
Hamim	54.300000	22.96667
IASBS	48.507111	36.70517
IER_Cinzana	-5.933867	13.27843
Ilorin	4.674500	8.48410
Issyk-Kul	76.983056	42.62278
Izana	-16.499060	28.30932
Jaipur	75.806217	26.90582
Kanpur	80.231639	26.51278
Karachi	67.135940	24.94574
La_Laguna	-16.321111	28.48194
Lake_Argyle	128.748500	-16.10810
Lampedusa	12.631667	35.51667
Mezaira	53.754660	23.10452
Mussafa	54.466667	24.37167
Muztagh	75.038764	38.40822
Nes_Ziona	34.789167	31.92250
Ouagadougou	-1.487230	12.42413
Ras_El_Ain	-7.599444	31.67028
SACOL	104.137083	35.94600
SEDE_BOKER	34.782222	30.85500
Saada	-8.155830	31.62583
Santa_Cruz_Tenerife	-16.247361	28.47253
Solar_Village	46.397286	24.90693
Tamanrasset	5.530000	22.79000
Tinga_Tingana	139.990933	-28.97583
Zinder_Airport	8.990233	13.77668